Transmitting Side Power Control for Dynamic Wireless Charging System of Electric Vehicles

Nguyen Kien Trung
School of Electrical and Electronic Engineering
Hanoi University of Science and Technology
Hanoi, Vietnam
trung.nguyenkien1@hust.edu.vn

Nguyen Thi Diep
Faculty of Control and Automation
Electric Power University
Hanoi, Vietnam
diepnt@epu.edu.vn

Received: 17 April 2022 | Revised: 25 June 2022 | Accepted: 29 June 2022

Abstract-This paper proposes a new power control method in dynamic wireless charging systems for electric vehicles. A dual-loop controller is proposed to control charging power while the electric vehicle is moving without communication between the transmitting and receiving sides. The output power is estimated through the coupling coefficient estimation. However, the coupling coefficient varies with the position of the vehicle. Therefore, this paper also presents an easy-to-do practical estimation method from the transmitting side, in which the coupling coefficient value is continuously updated according to the vehicle's position. As a result, the output power is controlled according to the required level with an error of less than 5%.

Keywords-electric vehicle; dynamic wireless charging; coupling coefficient estimation; LCC compensation; power control

I. INTRODUCTION

The use of Electric Vehicles (EVs) to reduce air pollution is globally rising. Much research on EVs is performed to make their use more convenient and safer [1-3]. One of the issues of interest to researchers is wireless charging technology for EVs [4, 5]. Wireless charging eliminates all charging cables, making charging safer and more flexible. Currently, Dynamic Wireless Charging (DWC) systems are preferred because EVs can be used on the road while charging [6, 7]. Therefore, the EVs can travel longer distances, the size and weight of the battery can be smaller, and the transportation efficiency is improved [8, 9]. In the DWC systems, output power pulses occur because coupling coefficients vary as the EVs move along the transmission lane. Moreover, output power sharply drops when the EV moves with lateral misalignment [10, 11]. This problem affects battery life. Many studies have been done to reduce the pulse of the output power by coil design [12, 13]. This solution may not be consistent for real EVs that have different sizes of receiver coil. In addition, these researches have not addressed the problem of EVs moving in lateral misalignment. Also, in a DWC system, many EVs of different types move and interact with the transmission lane and each EV type requires different levels of charging power [14]. Therefore, advanced control methods need to be applied in DWC systems to control the output power. Some studies perform power control for EVs in a wireless charging system [15]. In these studies, the output power is controlled using DC/DC converters on the receiving side. This solution increases the converters' number as well as increases the loss in the system.

This paper proposes a new power control method on the transmitting side without additional DC/DC converters. However, to be able to perform control only at the transmitting side, it is necessary to know the output power on the receiving side. The output power can be known by using the wireless communication network [16]. This solution is not suitable for the DWC system where the EVs are always moving in a hard environment. In [17], the transmitting-side inverter is also used to control the output power in DWC systems. This study uses auxiliary coils to detect the position of the EV and determines lateral misalignment to control the output power. This system takes up a lot of space and is expensive. In [18], parameters are estimated based on high-frequency voltage, current, and phase angle measurements. However, the method of measuring these parameters at high frequency is a challenge in practice. In [19], a quadrature transformation algorithm is used to estimate power. This method requires a complex measuring circuit and signal conversion. To solve the above difficulties, the current paper proposes an easy-to-do practical power estimation method based on measuring the resonant current RMS value on transmitter coils and inverter input DC power. This new power control method provides stable output power to any EV position and provides multi-level output power for different EV types in the DWC system.

II. THE POWER CONTROL PROBLEM

A. Structure of the Proposed System

The structure of the designed system is shown in Figure 1. On the transmitting side, transmitters are designed modular. Each module includes a full-bridge inverter that provides power to three transmitting coils through LCC compensation circuits. At the receiving side, the induced AC voltage on the receiving coil is also fed through the LCC compensation circuit to the impedance matching circuit, the battery management converter, and the battery. The transmitting coils are placed under the roadway to form a DWC lane for the EVs. In Figure 1, at the transmitting side: S_1 ~ S_4 is the SiC MOSFET; U_{DC},U_{AB} are input and output voltages of the inverter

Corresponding author: Nguyen Thi Diep

respectively, $L_{fi}, L_{fr}, C_{fi}, C_{fr}, C_i, C_r$ are the inductances, lower branch capacitors, and upper branch capacitors of double LCC compensation circuit respectively, I_i, I_{Li} are the input current to LCC compensation circuits and the resonant current on the transmitting coils (i=1,2,3) respectively, I_{Lr}, I_r, u_{ab} are the resonant current on the receiving coil, the output current/voltage of the compensation circuit, and L_i, L_r are the coil inductances. The issue of switching between modules has not been considered in this paper.

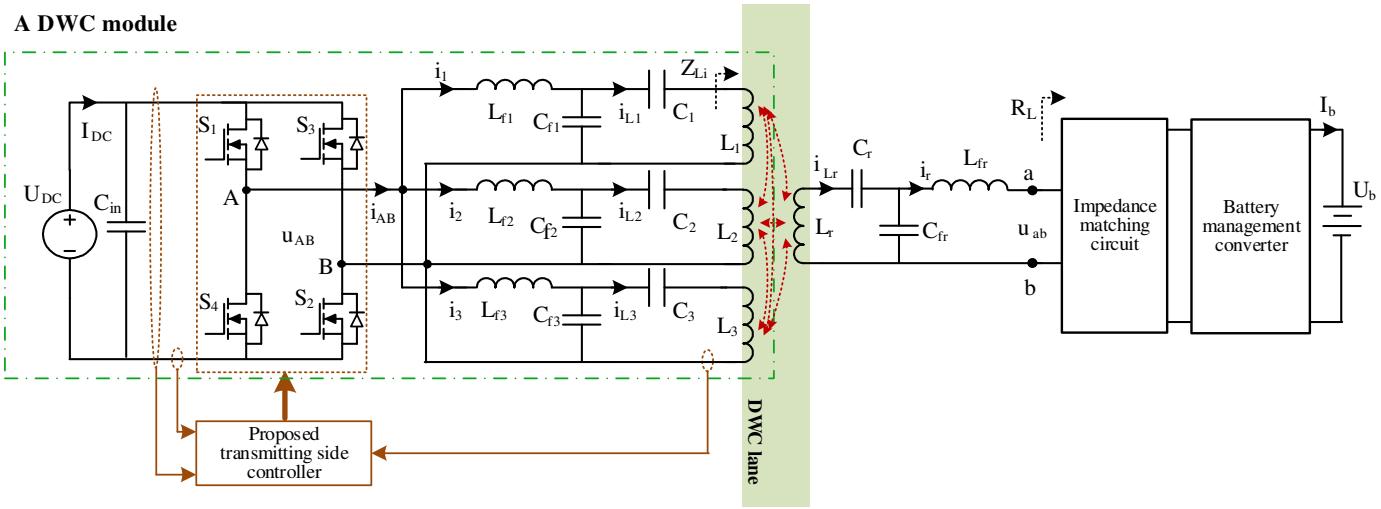

Fig. 1. The structure of the proposed DWC system.

B. *Characteristics of the Coupling Coefficient According to the EV's Position*

Figure 2 shows the FEA simulation model of a design system's magnetic coupler. The design of the transmitter and receiver is described in [20]. It is assumed that during dynamic charging, the transfer distance is always 150mm. Receiver's positions in the x and y directions are defined as dx and dy respectively. When the receiver is centered with the first transmitter (T_1), dx is zero and dy is zero. Figure 3 shows the FEA simulation result of the total coupling coefficient. This result is obtained in case dx increases from 0 to 800mm and dy increases from 0 to ±60mm, where the total coupling coefficient of the receiver with the transmitters is performed as follows:

$$k_r = \sum_{i=1}^{3} k_{ir} \quad (1)$$

where k_{ir} is the coupling coefficient of the ith transmitting coil (T_i) with the receiving coil (R). The results show that the coupling coefficient k_{ir} is the greatest when the receiving coil is centered with the transmitting coils.

The FEA simulation result in Figure 3 (solid lines) shows that when dy is 0mm (case 1-red line), the average value of the total coupling coefficient is 0.143. When dy is 40mm (case 2-blue line), the average value of the total coupling coefficient is 0.111. In case 3 (black line), the dy is 60mm and the average value of the total coupling coefficient is 0.078. These show that during dynamic charging, the total coupling coefficient is varied and is significantly reduced when lateral misalignment increases.

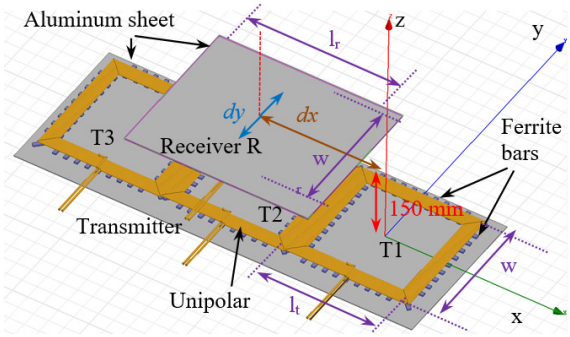

Fig. 2. The FEA model of the proposed magnetic coupler.

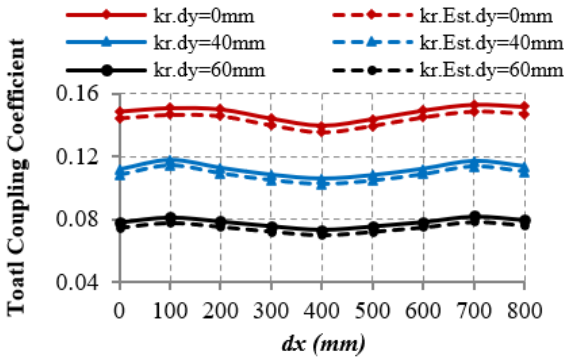

Fig. 3. FEA simulation/estimation coupling coefficients result.

C. *Analysis of Power Control Capability*

The fundamental harmonic approximation method was used to give an equivalent circuit as shown in Figure 4. U_{AB} is

approximated as a sinusoidal source. For simplicity in circuit analysis, the losses on the compensation circuit and inverter are ignored. R_i, R_r are the resistances of the transmitting and receiving coils respectively, R_L is the equivalent load impedance seen from the impedance matching circuit input to the load, $L_1 = L_2 = L_3 = L_i$ are the transmitting coils which are designed the same, M_i is the total mutual inductance of transmitting coil (L_i) with other transmitting coils ($M_i = \sum_{j=1, j\neq i}^{3} M_{ij}$), and M_{ir} is the mutual inductance of the transmitting coil (L_i) with the receiving coil (R).

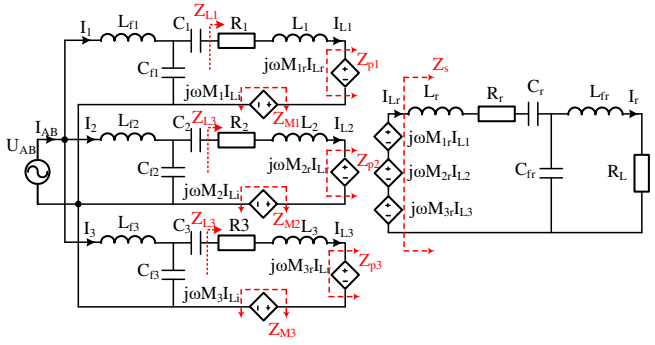

Fig. 4. Equivalent resonant circuit.

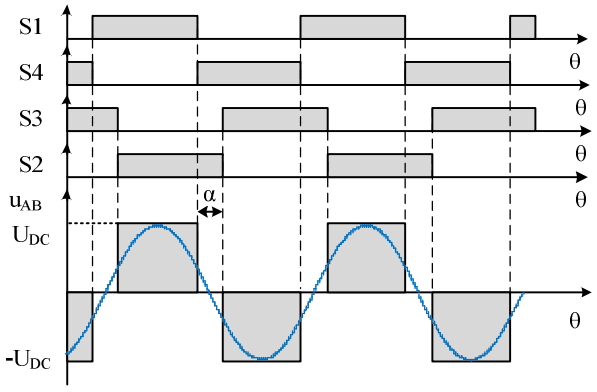

Fig. 5. The PWM signals for S1, S2, S3, S4, and voltage waveform.

The relationship of compensation circuit parameters is shown in (2) [20]:

$$\begin{cases} C_{fi} = \dfrac{1}{\omega^2 L_{fi}} \\ C_i = \dfrac{1}{\omega^2 (L_i - L_{fi} + M_i)} \\ C_{fr} = \dfrac{1}{\omega^2 L_{fr}} \\ C_r = \dfrac{1}{\omega^2 \left[L_r - L_{fr}\right]} \\ \omega = 2\pi f_{sw} \end{cases} \quad (2)$$

The resonant current in transmitting coils is the same and is expressed as [20]:

$$I_{L1} = I_{L2} = I_{L3} = I_{Li} = -j\omega C_{fi} U_{AB} \quad (3)$$

Analyzing the circuit of Figure 4 and combining it with (2)-(3) the output power can be expressed as:

$$P_{out} = \frac{R_L L_i L_r}{\left(\dfrac{R_r R_L}{\omega^2 L_{fr}} + L_{fr}\right)^2} k_r^2 I_{Li}^2 \quad (4)$$

In designed DWC systems, the resonant frequency is usually kept constant, and the designed parameters of coils and compensation circuits are constant. It is assumed that at the receiving side the equivalent load impedance value is maintained constant and equal to the optimal load value for maximum transfer efficiency. Equation (4) shows that if the coupling coefficient (k_r) is estimated, then the output power could be controlled by regulating the resonant current of transmitting coils (I_{Li}). Further, (3) shows that this resonant current can be controlled by controlling the inverter output voltage value (U_{AB}). The output voltage of the inverters is adjusted by the phase-shift method. The signals for S1~S4 and the inverter output voltage waveform are shown in Figure 5. The RMS of the inverter's output voltage can be expressed as [21]:

$$U_{AB} = \frac{2\sqrt{2}}{\pi} U_{DC} \cos\frac{\alpha}{2} \quad (5)$$

From (3), (4), and (5) it is shown that the output power can be adjusted by adjusting the phase-shift angle α.

D. Estimated Output Power

Given the circuit of Figure 4 at resonant point, the derivatives of the equations are shown below. The equivalent reflected impedance of transmitting coils to each other is:

$$Z_{Mi} = \frac{j\omega M_i I_{Li}}{I_{Li}} = j\omega M_i \text{ ; with } i = 1,2,3 \quad (6)$$

The receiving side impedance (Z_s) can be represented by the ratio between the coupled voltage $j\omega M_r I_{Li}$ and the receiver resonant current I_{Lr} as follows:

$$\begin{aligned} Z_s &= \frac{j\omega M_{1r} I_{L1} + j\omega M_{2r} I_{L2} + j\omega M_{3r} I_{L3}}{I_{Lr}} \\ &= \frac{j\omega \left(\sum_{i=1}^{3} M_{ir}\right) I_{Li}}{I_{Lr}} = \frac{j\omega M_r I_{Li}}{I_{Lr}} = R_r + \frac{\omega^2 L_{fr}^2}{R_L} \end{aligned} \quad (7)$$

The equivalent reflected impedance of the receiving coil to each transmitting coil can be expressed as:

$$Z_{pi} = \frac{j\omega M_{ir} I_{Lr}}{I_{Li}} = \frac{\omega^2 M_{ir} M_r}{Z_s} \quad (8)$$

The equivalent impedance of each transmitting coil is calculated as:

$$Z_{Li} = R_i + Z_{pi} + j\omega L_i + j\omega M_i \quad (9)$$

At the resonance condition, the reflected impedance Z_{pi} can be calculated as:

$$Z_{pi} = Re\{Z_{Li}\} - R_i = \frac{P_{Li}}{I_{Li.RMS}^2} - R_i \quad (10)$$

Approximately, ignoring the power loss on the inverter, the total impedance reflected from the secondary to the transmitting side is shown in (11):

$$\sum_{i=1}^{3} Z_{pi} = \frac{\sum_{i=1}^{3} P_{Li}}{I_{Li.RMS}^2} - 3R_i = \frac{P_{DC}}{I_{Li.RMS}^2} - 3R_i \quad (11)$$

where P_{DC} is the input power of the inverter. From (8) and (11), the coupling coefficient is given by:

$$k_r = \sqrt{\frac{1}{L_i L_r}\left[\frac{R_r}{\omega^2} + \frac{L_{fr}^2}{R_L}\right]\left[\frac{P_{DC}}{I_{Li.RMS}^2} - 3R_i\right]} \quad (12)$$

When the DWC system is designed, the system parameters, such as coils, compensator, and resonant angular frequency are assumed to be constant. When P_{DC} and $P_{Li.RMS}$ are measured by sensors, the equivalent load impedance (R_L) is maintained constant and k_r is estimated according to (12). Therefore, the output power is estimated according to (4).

E. The Proposed Power Controller

The block diagram of the proposed power controller is shown in Figure 6.

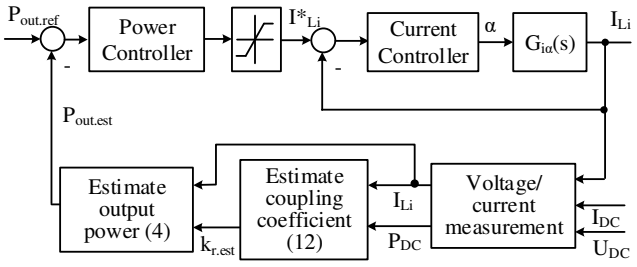

Fig. 6. Power control block diagram.

The inner loop is the current loop which is important for the estimated results to have high accuracy. The outer loop is a power control loop according to the load. At the transmitting side, the RMS value of resonant current (I_{Li}) and the value of the inverter input voltage/current (U_{DC} / I_{DC}) are measured. Then, (12) is used to estimate the coupling coefficient, and (4) is used to estimate the output power. The reference output power ($P_{out.ref}$) is compared with the estimated output power ($P_{out.est}$), then the error is taken to the power controller to determine the referent current value (I^*_{Li}). The error between the referent and the measured current is passed to the current controller. The current controller determines the phase shift angle to control the inverter.

III. SIMULATION AND EXPERIMENTAL RESULTS

A simulation model was built on PSIM simulation software to verify the proposed method. The system parameters are shown in Table I.

TABLE I. PARAMETERS OF THE DWC SYSTEM

Parameter	Values	Parameter	Values
P_{out}	1.5kW	L_{fi}	52.6μH
U_{DC}	310V	C_{fi}	66.5nF
U_{ab}	400V	C_1	93.7nF
k_r	0.14	C_2	123.2nF
f_{sw}	85kHz	C_3	95nF
L_i	102μH	L_{fr}	28.9μH
R_i	0.13Ω	C_{fr}	120.9nF
L_r	120μH	C_r	38.5nF
R_r	0.115Ω		

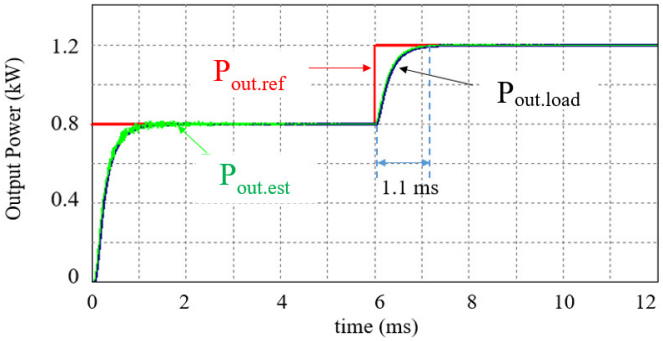

Fig. 7. Simulation characteristic of the output power according to the reference power.

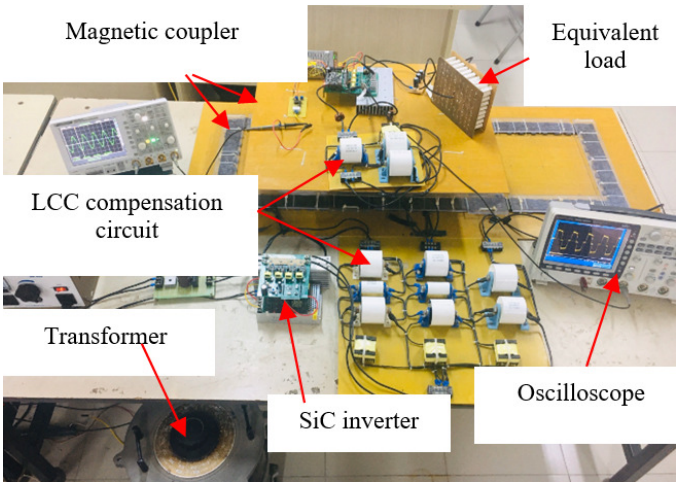

Fig. 8. The experimental DWC system setup.

The total coupling coefficient estimation results are shown in Figure 3(b) (dot lines). In case 1, dy is 0mm and the average value of the estimated total coupling coefficient ($K_{r.est}$) is equal to 0.138. In case 2, dy is 40mm and $K_{r.est}$ is equal to 0.108. In case 3, dy is 60mm and $K_{r.est}$ is equal to 0.074. The estimation error is less than 5.3%.

Figure 7 shows the simulation result of power control when the reference power changes from 0.8kW to 1.2kW. It shows that the value of the estimated power ($P_{out.est}$) and the load power ($P_{out.load}$) grip to the reference value ($P_{out.ref}$) with a response time of 1.1ms and an error of 0.5%. Figure 8 shows the experimental model of the proposed DWC system. PE40 ferrite bars were used to increase magnetic conductivity. Polypropylene film capacitors were used for their small loss and high ability to withstand high currents at high frequencies. MOSFETs SiC (C3M0280090D) was used for the inverter. Stranded wire was used in building the coils. The impedance matching circuit and battery were replaced by an equivalent load.

The experimental waveforms when the receiver position dx and dy are zero and $U_{DC} = 310V$ are presented in Figure 9. The results show that the resonant frequency is 85kHz and the ZVS condition for SiC is achieved in both cases of phase shift angle (α) equal to 0 and 60^0. Figure 9(a) shows the resonant current $I_{Li} = 10.6A$, output power equal to 1.32kW, and the system efficiency reaching 89.6% in the case of $\alpha = 0^0$. Figure 9(b) shows that when $\alpha = 60^0$, $I_{Li} = 9.2A$, the output power is equal to 1.2kW and the system efficiency reaches 89.2%.

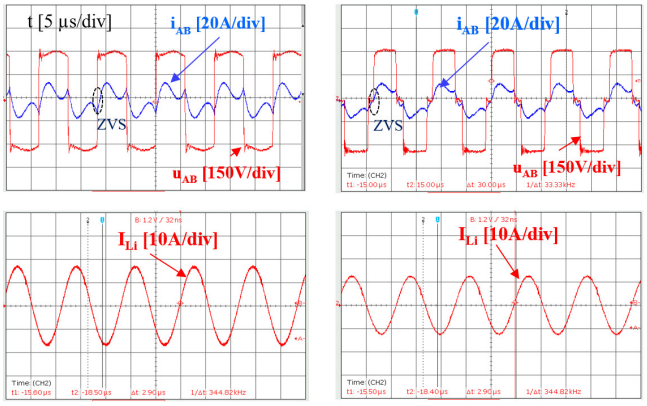

(a) $\alpha = 0^0$ (b) $\alpha = 60^0$

Fig. 9. Experimental waveforms: inverter output voltage/current and resonant currents.

The following tests were performed to demonstrate the operation of the dual-loop controller in two cases. The DC voltage (U_{DC}) was set to 250V and the equivalent load R_L to 53.3Ω. In case 1, when the position of the receiver is $dx = 0$mm to 800mm and dy = 0mm, the required output power changes from 600W to 400W. The experimental results of the reference/ estimation/measured output power, phase shift angle α, the inverter output voltage waveform (u_{AB} - red color), and resonant current (I_{Li} - blue color) are presented in Figure 10. The results show that the angle α increased from 41.6 to 51.4^0, $I_{Li.RMS}$ decreased from 6.34A to 5.21A, and the output power responds to the preset value. In case 2, when the position of the receiver is a lateral misalignment in the y-direction from 0mm to 40mm, the reference output power is 400W. The experimental results are presented in Figure 11. In this case, the coupling coefficient reduces, the phase shift angle α decreased from 52.6 to 36.7^0, the r.m.s value of I_{Li} increased from 5.18A to 6.9A, and the output power was constant.

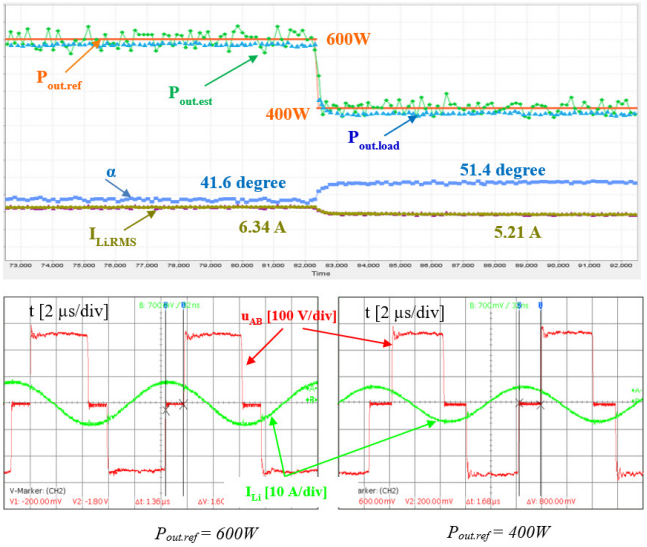

$P_{out.ref} = 600W$ $P_{out.ref} = 400W$

Fig. 10. Experimental results when the reference output power changes from 600W to 400W.

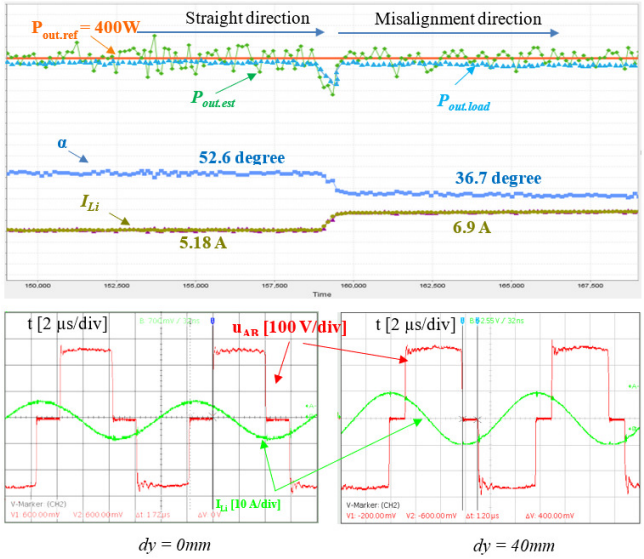

$dy = 0mm$ $dy = 40mm$

Fig. 11. Experimental results when the reference output power is 400W.

These results show that the proposed control method could control the output power with a response time of 0.01s and an error less than 5%. The output power estimation method could continuously estimate the output power. The proposed system responds well when the vehicle speed is below 40km/h. Figure 12 shows the system's efficiency experimental result when the

receiver moves along the transmission lane without any lateral misalignment. The average system efficiency is 80.7%.

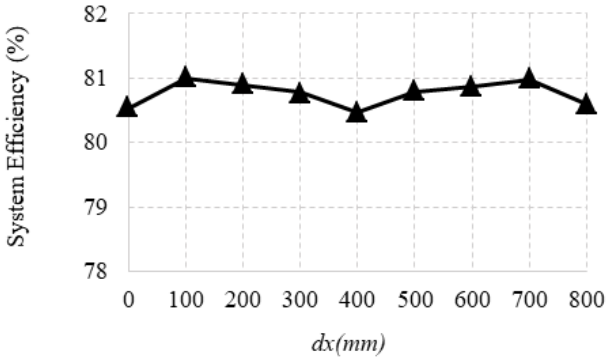

Fig. 12. Experimental efficiency characteristics.

IV. CONCLUSION

This paper proposes a new method of controlling the output power in the DWC system for EVs. The transmitting side inverter has been used to control power without using an additional boost/buck inverter. The parameter estimation method has been made simple by measuring the r.m.s. value of the sinusoidal current and the DC input power of the inverter. These solutions can lower the cost of the system. Furthermore, the proposed method can control the output power according to the required level of different EVs. The average system efficiency reaches 80.7%. The output power is controlled in the DWC with an error less than 5%.

REFERENCES

[1] G. A. Covic and J. T. Boys, "Modern Trends in Inductive Power Transfer for Transportation Applications," *IEEE Journal of Emerging and Selected Topics in Power Electronics*, vol. 1, no. 1, pp. 28–41, Mar. 2013, https://doi.org/10.1109/JESTPE.2013.2264473.

[2] M. Hussain, A. Ulasyar, H. S. Zad, A. Khattak, S. Nisar, and K. Imran, "Design and Analysis of a Dual Rotor Multiphase Brushless DC Motor for its Application in Electric Vehicles," *Engineering, Technology & Applied Science Research*, vol. 11, no. 6, pp. 7846–7852, Dec. 2021, https://doi.org/10.48084/etasr.4345.

[3] V. K. B. Ponnam and K. Swarnasri, "Multi-Objective Optimal Allocation of Electric Vehicle Charging Stations and Distributed Generators in Radial Distribution Systems using Metaheuristic Optimization Algorithms," *Engineering, Technology & Applied Science Research*, vol. 10, no. 3, pp. 5837–5844, Jun. 2020, https://doi.org/10.48084/etasr.3517.

[4] S. Li and C. C. Mi, "Wireless Power Transfer for Electric Vehicle Applications," *IEEE Journal of Emerging and Selected Topics in Power Electronics*, vol. 3, no. 1, pp. 4–17, Mar. 2015, https://doi.org/10.1109/JESTPE.2014.2319453.

[5] M. E. Bendib and A. Mekias, "Solar Panel and Wireless Power Transmission System as a Smart Grid for Electric Vehicles," *Engineering, Technology & Applied Science Research*, vol. 10, no. 3, pp. 5683–5688, Jun. 2020, https://doi.org/10.48084/etasr.3473.

[6] S. Lukic and Z. Pantic, "Cutting the Cord: Static and Dynamic Inductive Wireless Charging of Electric Vehicles," *IEEE Electrification Magazine*, vol. 1, no. 1, pp. 57–64, Sep. 2013, https://doi.org/10.1109/MELE.2013.2273228.

[7] L. A. Maglaras, F. V. Topalis, and A. L. Maglaras, "Cooperative approaches for dymanic wireless charging of Electric Vehicles in a smart city," in *2014 IEEE International Energy Conference (ENERGYCON)*, Cavtat, Croatia, Feb. 2014, pp. 1365–1369, https://doi.org/10.1109/ENERGYCON.2014.6850600.

[8] S. Chopra and P. Bauer, "Driving Range Extension of EV With On-Road Contactless Power Transfer—A Case Study," *IEEE Transactions on Industrial Electronics*, vol. 60, no. 1, pp. 329–338, Jan. 2013, https://doi.org/10.1109/TIE.2011.2182015.

[9] A. Shekhar, M. Bolech, V. Prasanth, and P. Bauer, "Economic considerations for on-road wireless charging systems - A case study," in *2015 IEEE PELS Workshop on Emerging Technologies: Wireless Power (2015 WoW)*, Daejeon, Korea (South), Jun. 2015, https://doi.org/10.1109/WoW.2015.7132804.

[10] O. C. Onar, J. M. Miller, S. L. Campbell, C. Coomer, Cliff. P. White, and L. E. Seiber, "A novel wireless power transfer for in-motion EV/PHEV charging," in *2013 Twenty-Eighth Annual IEEE Applied Power Electronics Conference and Exposition (APEC)*, Long Beach, CA, USA, Mar. 2013, pp. 3073–3080, https://doi.org/10.1109/APEC.2013.6520738.

[11] Q. Zhu, L. Wang, Y. Guo, C. Liao, and F. Li, "Applying LCC Compensation Network to Dynamic Wireless EV Charging System," *IEEE Transactions on Industrial Electronics*, vol. 63, no. 10, pp. 6557–6567, Jul. 2016, https://doi.org/10.1109/TIE.2016.2529561.

[12] F. Lu, H. Zhang, H. Hofmann, and C. C. Mi, "A Dynamic Charging System With Reduced Output Power Pulsation for Electric Vehicles," *IEEE Transactions on Industrial Electronics*, vol. 63, no. 10, pp. 6580–6590, Jul. 2016, https://doi.org/10.1109/TIE.2016.2563380.

[13] V.-B. Vu, M. Dahidah, V. Pickert, and V.-T. Phan, "A High-Power Multiphase Wireless Dynamic Charging System With Low Output Power Pulsation for Electric Vehicles," *IEEE Journal of Emerging and Selected Topics in Power Electronics*, vol. 8, no. 4, pp. 3592–3608, Sep. 2020, https://doi.org/10.1109/JESTPE.2019.2932302.

[14] M. Yilmaz and P. T. Krein, "Review of Battery Charger Topologies, Charging Power Levels, and Infrastructure for Plug-In Electric and Hybrid Vehicles," *IEEE Transactions on Power Electronics*, vol. 28, no. 5, pp. 2151–2169, Feb. 2013, https://doi.org/10.1109/TPEL.2012.2212917.

[15] M. Kim, D.-M. Joo, and B. K. Lee, "Design and Control of Inductive Power Transfer System for Electric Vehicles Considering Wide Variation of Output Voltage and Coupling Coefficient," *IEEE Transactions on Power Electronics*, vol. 34, no. 2, pp. 1197–1208, Oct. 2019, https://doi.org/10.1109/TPEL.2018.2835161.

[16] E. Gati, G. Kampitsis, and S. Manias, "Variable Frequency Controller for Inductive Power Transfer in Dynamic Conditions," *IEEE Transactions on Power Electronics*, vol. 32, no. 2, pp. 1684–1696, Oct. 2017, https://doi.org/10.1109/TPEL.2016.2555963.

[17] R. Tavakoli and Z. Pantic, "Analysis, Design, and Demonstration of a 25-kW Dynamic Wireless Charging System for Roadway Electric Vehicles," *IEEE Journal of Emerging and Selected Topics in Power Electronics*, vol. 6, no. 3, pp. 1378–1393, Sep. 2018, https://doi.org/10.1109/JESTPE.2017.2761763.

[18] V. Jiwariyavej, T. Imura, and Y. Hori, "Coupling Coefficients Estimation of Wireless Power Transfer System via Magnetic Resonance Coupling Using Information From Either Side of the System," *IEEE Journal of Emerging and Selected Topics in Power Electronics*, vol. 3, no. 1, pp. 191–200, Mar. 2015, https://doi.org/10.1109/JESTPE.2014.2332056.

[19] K. Song, Z. Li, J. Jiang, and C. Zhu, "Constant Current/Voltage Charging Operation for Series–Series and Series–Parallel Compensated Wireless Power Transfer Systems Employing Primary-Side Controller," *IEEE Transactions on Power Electronics*, vol. 33, no. 9, pp. 8065–8080, Sep. 2018, https://doi.org/10.1109/TPEL.2017.2767099.

[20] N. T. Diep, N. K. Trung, and T. T. Minh, "Wireless power transfer system design for electric vehicle dynamic charging application," *International Journal of Power Electronics and Drive Systems (IJPEDS)*, vol. 11, no. 3, pp. 1468–1480, Sep. 2020, https://doi.org/10.11591/ijpeds.v11.i3.pp1468-1480.

[21] Z. Ye, P. K. Jain, and P. C. Sen, "A Full-Bridge Resonant Inverter With Modified Phase-Shift Modulation for High-Frequency AC Power Distribution Systems," *IEEE Transactions on Industrial Electronics*, vol. 54, no. 5, pp. 2831–2845, Jul. 2007, https://doi.org/10.1109/TIE.2007.896030.